AIAA SciTech Forum
8-12 January 2024, Orlando, FL
AIAA SCITECH 2024 Forum

10.2514/6.2024-2498

Measurements of NO Rotational and Vibrational Temperatures Behind a Normal Shock in Hypervelocity Flow via Absorption Spectroscopy

Samuel E. Feltis[1] and Zhili Zhang[2]
University of Tennessee, Knoxville, TN, 37996, U.S.A.

Tyler S. Dean[3] and Rodney D.W. Bowersox[4]
Texas A&M University, College Station, TX, 77834, U.S.A.

Farhan Siddiqui[5] and Mark Gragston[6]
University of Tennessee, Knoxville, TN, 37996, U.S.A.
University of Tennessee Space Institute, Tullahoma, TN, 37388, U.S.A.

Tunable Diode Laser Absorption Spectroscopy (TDLAS) measurements of nitric oxide (NO) in the vicinity of 5.26 µm were conducted in the Texas A&M Hypervelocity Expansion Tunnel (HXT). Path-averaged flow parameters of rotational and vibrational temperatures and NO concentration at a measurement rate of 30 kHz were obtained. Thermal nonequilibrium and NO concentration levels in the post-shock region were measured. Measurements are compared to equilibrium calculations. The experimental measurements of the rotational temperature show a consistent value up to 3000 K larger than the calculated equilibrium values. Similarly with the vibrational temperature, the measurements resulting from the experimental data are between 1000 to 3000 K colder than the equilibrium results. The NO concentrations in all runs are near to the reported equilibrium value; often beginning higher than, and over time decaying to, the equilibrium concentration value of the specific tunnel run.

I. Nomenclature

α	=	Absorbance
c_2	=	2nd radiation constant
ΔF	=	Change in rotational energy
ΔG	=	Change in vibrational energy
F''	=	Lower-state rotational energy
G''	=	Lower-state vibrational energy
I_t	=	Transmitted signal
I_0	=	Baseline signal

[1] Graduate Research Assistant, Department of Mechanical, Aerospace, and Biomedical Engineering
[2] Professor, Department of Mechanical, Aerospace, and Biomedical Engineering, AIAA Associate Fellow
[3] Graduate Research Assistant, Department of Aerospace Engineering, Texas A&M University, Student Member AIAA
[4] Professor, Aerospace Engineering; Associate Dean for Research; Regents Professor; Holder, Ford I Professorship; AIAA Fellow
[5] Post-Doctoral Research Associate, HORIZON Research Group, AIAA Member
[6] Assistant Professor, Department of Mechanical, Aerospace, and Biomedical Engineering, AIAA Member

L	=	Laser pathlength
n	=	Molecular density
S	=	Linestrength intensity
σ	=	Absorption cross-section
T_x	=	Temperature of x mode excitation
τ	=	Transmission

II. Introduction

Strong shockwaves are ubiquitous in hypersonic flight conditions, and the increase in gas temperature through such strong compressions can result in the generation of nitric oxide (NO), the activation of vibrational energy modes of molecules, and possibly dissociation chemistry depending on the flow conditions. The molecular dissociation and redistribution of energy among the available vibrational energy modes leads to changes in the physical and transport properties of the gas that have a significant impact on the calculation of important engineering quantities, such as the amount of surface heat transfer [1, 2]. As ground testing facilities are key to development of hypersonic flight systems, it is important to quantify these high-temperature gas effects during testing.

In this work, NO that formed behind a normal shock in a Mach 8.5 flow was analyzed via tunable diode laser absorption spectroscopy (TDLAS) to recover the rotational and vibrational temperatures. A two-temperature model is used to understand the effect on nonequilibrium flow behind the shockwave. Similar assumptions were also made in work by Girard et al [1]. Furthermore, all excited states are presumed to be in the $X^2\Pi$ ground state of NO, allowing for the approximation of a constant electronic partition function, removing the need to consider the electronic temperature [2]. This work was primarily focused on establishing a baseline analysis for TDLAS in the Texas A&M Hypervelocity Expansion Tunnel (HXT), with future interest focusing on measuring thermochemical nonequilibrium in the shear flow region of a Mach stem interaction.

III. Experimental Setup

a. Facility and Test conditions

Experiments were done in the HXT which is described in detail by Dean et al. 2022 [3] and depicted in Fig. 1. The 30.5 m long facility features 0.48 m diameter pipe in the driver, driven, and expansion sections and a nozzle with 0.92 m exit diameter is used to further expand the flow to achieve increased Mach number range, test-time, and test core size.

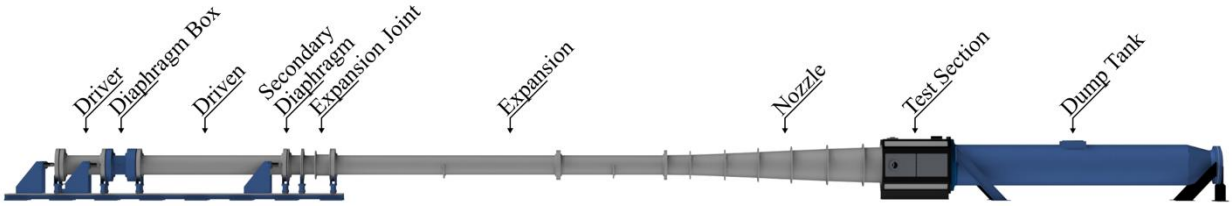

Figure 1: The components of the Texas A&M HXT facility [3].

In each test helium was used for the driver gas while air was used in the driven section.

b. Model Geometry

The model geometry used in this work is described by Dean et al. 2023 [4] and shown in Fig. 2. Measurements were carried out at approximately 30 mm behind the resulting normal shock region. The normal shock is well illustrated in Fig. 2.

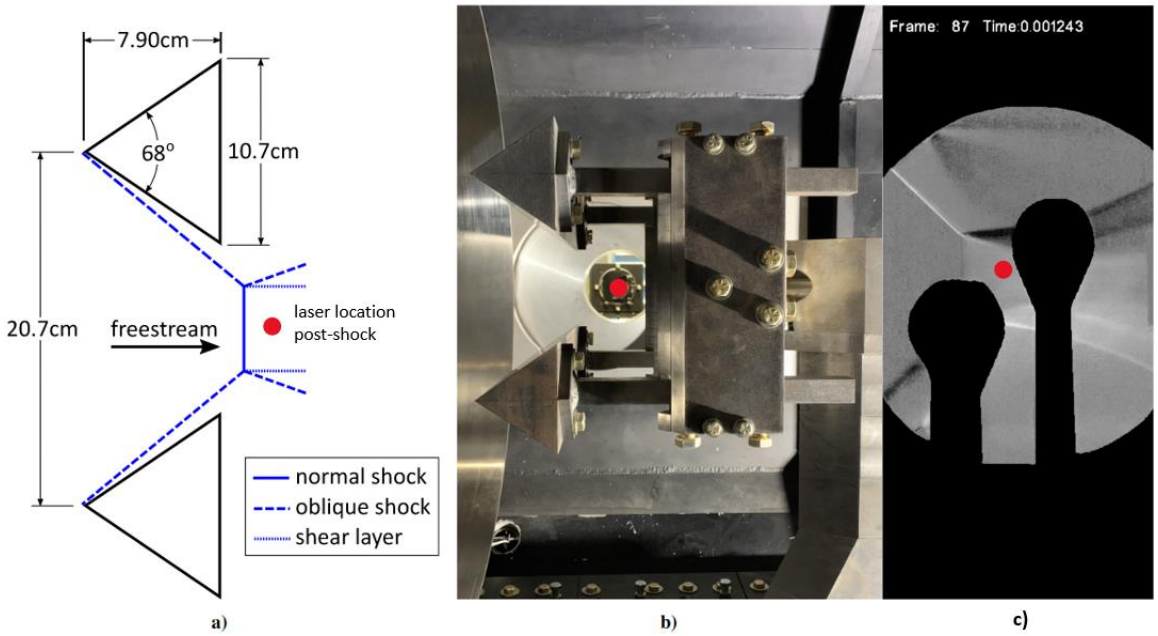

Figure 2: (a) Dimensioned drawing of the Mach stem generator with representative flow structures and laser location, (b) a photograph as installed in the HXT test-section (viewed from the side), and (c) Schlieren image visualizing Mach stems in steady state from run 221 (with mirrors for NO and atomic oxygen silhouetted).

Equilibrium conditions of the flow in this region are shown in Table 1. These calculations were done assuming a 7-species model using the JANAF thermochemical data [5].

HXT Run Number	E.Q. T_2 [K]	E.Q. p_2 [kPa]	E.Q. ρ_2 [kg/m^3]	E.Q. NO Mole Fraction	E.Q. NO Mass Fraction
219	3780	107.94	0.0888	0.049	0.057
220	4931	15.42	0.0087	0.008	0.010
221	4285	40.85	0.0282	0.023	0.028
222	4285	40.85	0.0282	0.023	0.028

Table 1: Equilibrium conditions for the post-normal shock region.

c. Tunable Diode Laser Absorption Spectroscopy Setup

A schematic showing the beam path of the diode laser beam is shown in Fig. 3. The 5.26 μm beam was guided into the tunnel using a silver mirror and then turned onto a detector using another silver mirror. A bandpass filter was placed in front of the detector to reduce any potential contributions from other light sources. The laser current was modulated at 30 kHz to perform the necessary wavelength sweeping on a timescale comparable to the facility run time.

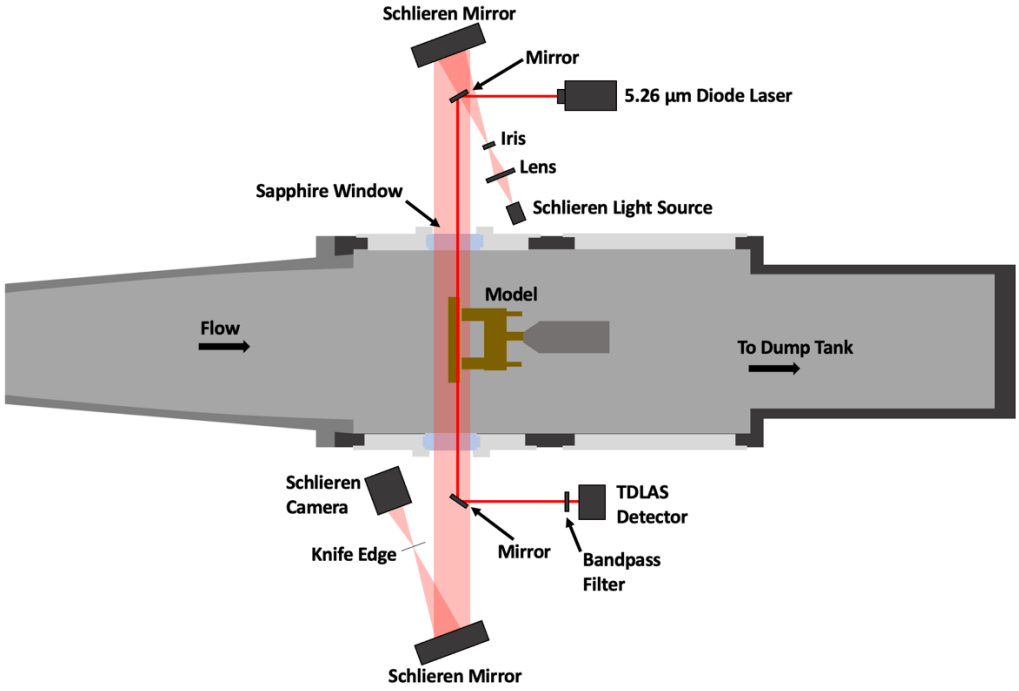

Figure 3: A diagram showing the beam path of the diode laser beam with respect to the tunnel and model as well as the concurrent schlieren setup.

IV. Ro-Vibrational Model

A ro-vibrational temperature (RVT) model was created for the better understanding of how NO changes in both rotational and vibrational temperature. The translational temperature is assumed to be equal to that of the rotational while the electronic temperature component is considered negligible. Beginning with the foundation of absorption spectroscopy, the Beer-Lambert Law, write,

$$\frac{I_t}{I_0} = e^{-\alpha} = \tau = \sum_i \tau_i$$
$$\tau_i = e^{-n\sigma_i L} \tag{1}$$

Where I_t is the transmitted signal through the absorbing medium and I_0 is the baseline, the signal with no absorbing species present. The ratio of these two signals relates the absorbance α to the experimental data. The transmission τ is a function of the molecular density n in cm^{-3}, the absorption cross-section σ in cm^2, and the pathlength L in cm. The linestrength intensity is required to calculate the absorption cross section. This is given by Eq. (2), modified from HITRAN for the separation of assumed equilibrium temperature into rotational and vibrational components. The units of the linestrength intensity S are given in $cm^{-1}/(molecule \cdot cm^{-2})$.

$$S_i(T_r, T_v) = S_i(T_0)\frac{Q(T_0, T_0)}{Q(T_r, T_v)}\exp\left[-c_2\left(\frac{F_i''}{T_r} + \frac{G_i''}{T_v} - \frac{F_i'' + G_i''}{T_0}\right)\right]\frac{1 - \exp\left[-c_2\left(\frac{\Delta F_i}{T_r} + \frac{\Delta G_i}{T_v}\right)\right]}{1 - \exp\left[-\frac{c_2(\Delta F_i + \Delta G_i)}{T_0}\right]} \tag{2}$$

Where the partition function Q is taken from Hanson [2]. The energies are found from the 1992 work of J. Reisel et al. [6]. Shown in Fig. 4 are the results of this model.

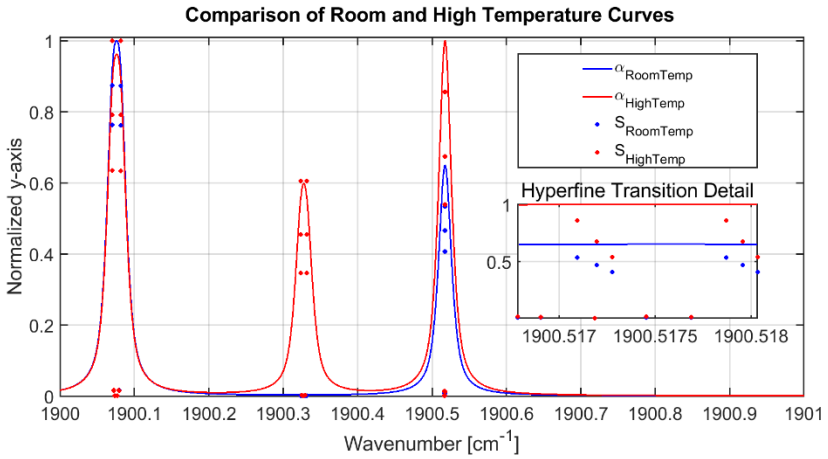

Figure 4: Comparison of two modeled absorbance curves and two sets of linestrength intensities at room temperature ($T_r = T_v = 296\ K$) and high temperature ($T_r = T_v = 1500\ K$) across transitions of NO.

The two absorbance curves in Fig. 4 (labeled $\alpha_{RoomTemp}$ and $\alpha_{HighTemp}$) show how the model responds to different temperature inputs maintaining the NO concentration and the pressure constant at 0.02 mole fraction and 0.4 atm. The two curves have been normalized for ease of comparison. Alongside either of the curves are the corresponding normalized linestrength intensities $S_{RoomTemp}$ and $S_{HighTemp}$ taken via Eq. (2) for the same temperatures as the absorbance curves.

The data are fit to recover the two temperature values through an iterative technique. The data are taken from an oscilloscope, both the transmitted signal and the baseline, and analyzed in MATLAB using Eq. (1); the signals are shown in Fig. 5 with the vibrational and rotational bands shown in Fig. 6. They are broken into up-cycles and down-cycles dependent on whether they occur on the rise or the fall of the carrying sinewave. The periodic cycles were not averaged so as to better preserve the shape of each spectrum in time.

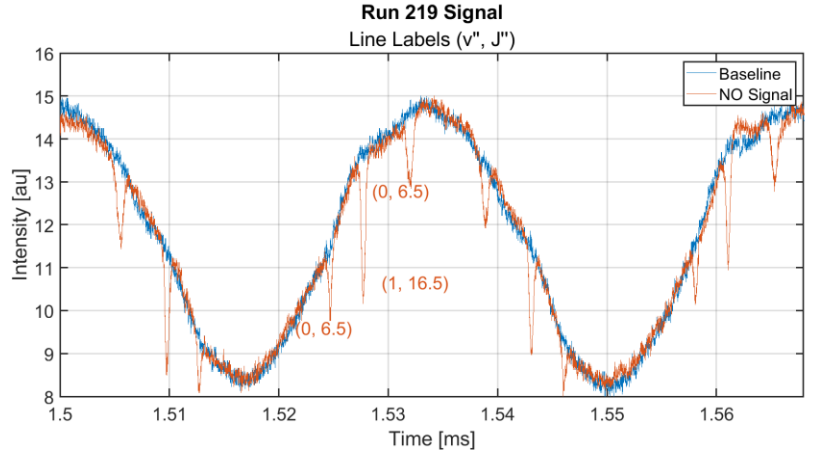

Fig. 5: Baseline signal and transmitted NO signal from Run 219.

Each signal is analyzed independently with starting conditions equal to the equilibrium values shown in Table 1.

V. Experimental Results

The four runs tested in the HXT were fitted with the above method. Most of the fits are well natured yielding minimal percent errors throughout. Shown in Fig. 6 in black are the experimental data and in red is the RVT model fit for run 219.

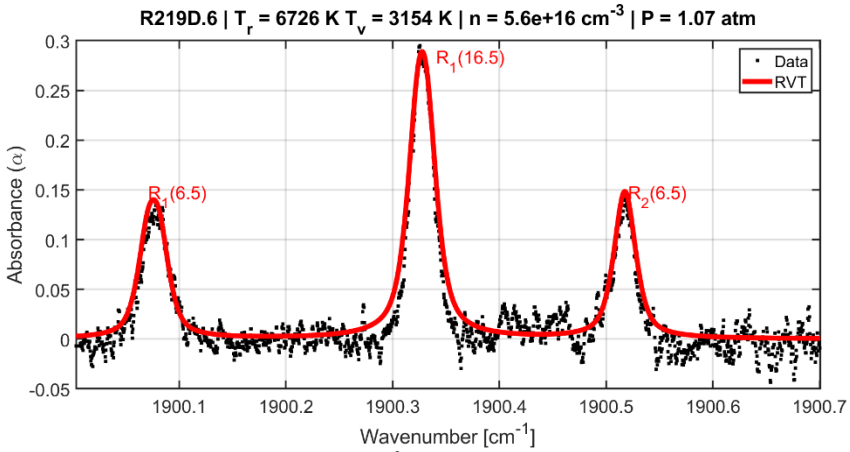

Figure 6: Run 219, 6th down-cycle measurement.

As the steady state began to decay toward the later periodic cycles, the signal to noise ratio diminished greatly as shown in Fig. 7. Therefore, the data just prior to the end of steady state have been discarded.

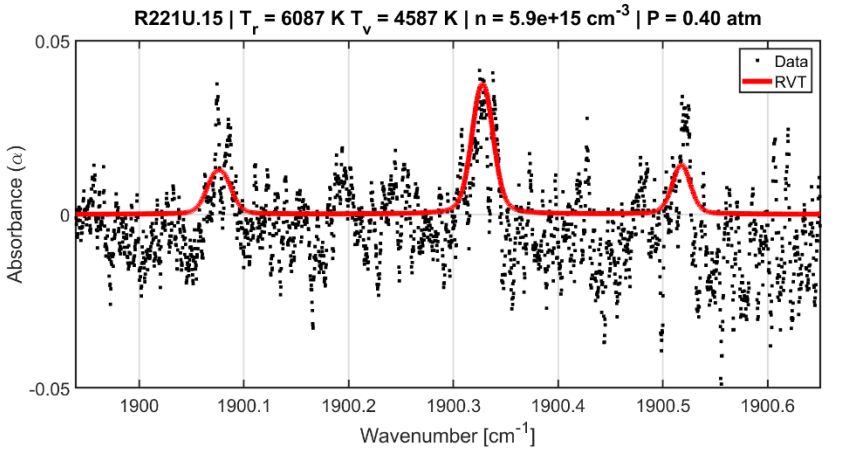

Figure 7: Best fit for noisy, low-concentration NO data in run 221, 15th up-cycle measurement.

As the noise level reached the measured height value of the peaks, it became difficult to accurately model the temperature and the concentration of NO present in the system. This is reflected in Fig. 10 where the NO concentration tapers off toward the end of the steady state conditions.

Figure 8 shows the recovered rotational and vibrational temperatures from run 219 as well as the trendlines of either. The uncertainty bounds of each datapoint are taken from Eq. (3), the maximum of the absolute percent error.

$$MAPE = \text{maximum}\left[\left|\frac{\tau_{sim} - \tau_{exp}}{\tau_{exp}}\right| \times 100\right] \tag{3}$$

Where τ_{sim} is the transmission of the simulated model and τ_{exp} is the transmission of the experimental data. These are found in the manner shown in Eq. (1) as just the exponential of the negative absorbance α.

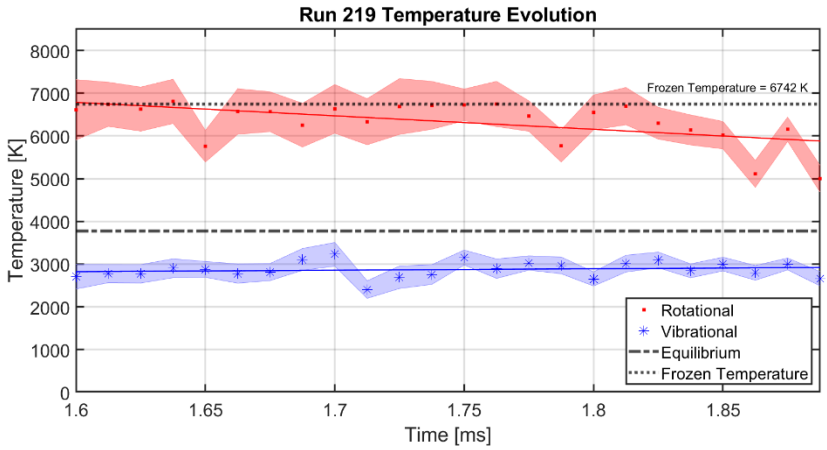

Figure 8: Temperature evolution across run 219.

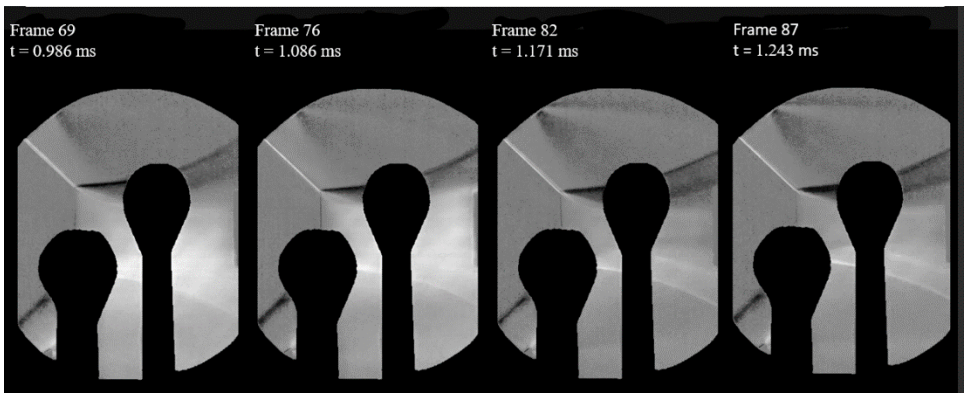

Figure 9: Schlieren images throughout steady state of run 221 from 0.986 to 1.243 ms with beam-posts for NO and atomic oxygen detection silhouetted.

To note, throughout any given run there would be occasional disturbances or fluctuations in the post-shock region as illustrated by the opaqueness of the flow in frames 69 and 76 of Fig. 9. Fluctuations like these are likely what causes the oscillations in the temperature and concentration data in Figs. 8 and 10.

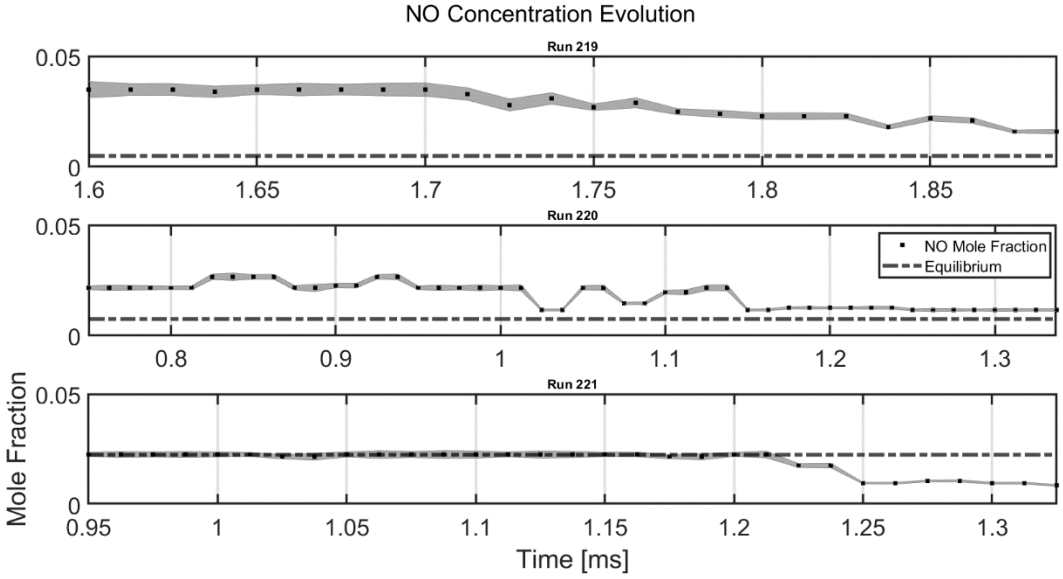

Figure 10: Concentration changes for NO across steady state for three of the runs of the HXT.

VI. Conclusions

TDLAS, alongside an RVT model of NO, has been utilized to characterize the rotational and vibrational temperature evolution, as well as the concentration evolution of flow behind a normal shock in an expansion tunnel. From the measurable wavelengths of the IR laser, only NO was measured with negligible interference from other molecular species. These measurements were temporally resolved to provide progression data for rotational and vibrational temperature as well as NO concentration during the approximately 1 ms run time for the facility. From the data and the methodology described in this paper, it is shown that the rotational and vibrational temperatures while under steady state conditions for the HXT do not converge or decay quickly and are slightly stable around the starting conditions. Likewise, the concentration of NO in the system for the duration of steady state is consistent until the degradation of steady state begins. In total, most of the test conditions show thermal nonequilibrium between the vibrational and rotational energy states for NO behind the normal shock. Future work will seek to replicate and add on to these data for the more complete quantification of high enthalpy flows and characterization of the HXT.

VII. Acknowledgements

The authors gratefully acknowledge the Office of the Under Secretary of Defense Vannevar Bush Faculty Fellowship program (Drs. B. Nair and J. Cambier, N00014-18-1-3020) for sponsoring a portion of this study. Its contents are solely the responsibility of the authors and do not necessarily represent the official views of the Department of Defense. The authors also acknowledge support from the National Science Foundation under NSF-2026242 and the DOE under DE-SC0021382.

References

[1] Girard, J. J., Finch, P. M., Strand, C. L., Hanson, R. K., Yu, W. M., Austin, J. M., and Hornung, H. G., "Measurements of Reflected Shock Tunnel Freestream Nitric Oxide Temperatures and Partial Pressure," *AIAA Journal*, Vol. 59, No. 12, 2021, pp. 5266–5275. https://doi.org/10.2514/1.J060596

[2] Hanson, R. K., Spearrin, R. M., and Goldenstein, C. S., "Spectroscopy and Optical Diagnostics for Gases," Springer International Publishing, Cham, 2016. https://doi.org/10.1007/978-3-319-23252-2

[3] Dean, T., Blair, T. R., Roberts, M., Limbach, C., and Bowersox, R. D., "On the Initial Characterization of a Large-Scale Hypervelocity Expansion Tunnel," *AIAA SCITECH 2022 Forum*, American Institute of Aeronautics and Astronautics. https://doi.org/10.2514/6.2022-1602

[4] Dean, T., Siddiqui, F., Gragston, M. T., and Bowersox, R. D., "Index of Refraction Fluctuation Spectra in Aerothermochemical Non-Equilibrium Shock Layers," *AIAA SCITECH 2023 Forum*, American Institute of Aeronautics and Astronautics, 2023. https://doi.org/10.2514/6.2023-0270

[5] Chase, M. J., "NIST-JANAF Thermochemical Tables, Monograph 9," American Chemical Society, Washington DC.

[6] Reisel, J. R., Carter, C. D., and Laurendeau, N. M., "Einstein Coefficients for Rotational Lines of the (0, 0) Band of the NO A2Σ+-X2π System," *Journal of Quantitative Spectroscopy and Radiative Transfer*, Vol. 47, No. 1, 1992, pp. 43–54. https://doi.org/10.1016/0022-4073(92)90078-I